Low temperature in situ formation of cobalt in silicon nitride toward functional nitride nanocomposites †

Shotaro Tada, Maira Debarba Mallmann, Haruna Takagi, Junya Iihama, Norifumi Asakuma, Toru Asaka, Yusuke Daiko, Sawao Honda, Rafael Kenji Nishihora, Ricardo Antonio Francisco Machado, et al.

Cite this: DOI: 10.1039/d0cc07366k

Low temperature *in situ* formation of cobalt in silicon nitride toward functional nitride nanocomposites†

Shotaro Tada, [a] Maira Debarba Mallmann,[bc] Haruna Takagi,[a] Junya Iihama,[a] Norifumi Asakuma,[a] Toru Asaka,[a] Yusuke Daiko, [a] Sawao Honda,[a] Rafael Kenji Nishihora,[bc] Ricardo Antonio Francisco Machado,[c] Samuel Bernard [b] and Yuji Iwamoto *[a]

This work highlights the first demonstration of a low-temperature *in situ* formation of Co nanocrystallites embedded within an amorphous silicon nitride matrix through careful control of the chemistry behind material design using perhydropolysilazane (PHPS) as a Si_3N_4 precursor further coordinated with $CoCl_2$ and ammonia as a pyrolysis atmosphere. The Co nucleation was allowed to proceed at temperatures as low as 400 8C *via* thermal decomposition of Co_2N pre-formed *in situ* by the reaction of $CoCl_2$ with the Si centers of PHPS at the early stage of pyrolysis (220–350 8C).

Material discovery is a key element in the innovation cycle of energy conversion, transmission and storage technologies.[1] In this category of energy-focused materials, advanced ceramics appear to be high value-added products with performances that are tailored *via* their rational and elaborate designs.[2–6] Ceramic processing methods based on molecular engineering and precursor chemistry are well appropriate approaches to design such materials that can reach performances far beyond those developed by more conventional synthesis routes.[7–10] A very convenient precursor route is the polymer derived ceramics (PDCs) route which allows fine control over the chemical composition of the final ceramic materials as well as their phase distribution and nanostructure.[11,12] This offers enhanced or novel functional properties which have been recently highlighted in metal/Si-based (oxy-)carbide and carbonitride matrix composites such as Ni/SiC,[13] Ni/SiOC,[14] Ni/SiCN(O)[15] and M/SiCN (M = Pd,[16] Ru,[16] Pd_2Ru,[17] Cu,[18,19] Ir,[16,20] Ni,[21] Pt,[22,23] Co,[24] Fe[25]) derived from metal-modified polycarbosilanes, polysiloxanes and polysilazanes, respectively. In particular, as reported by Kempe *et al.*, the polymer-derived M/SiCN nanocomposites are attractive as robust and reusable catalysts which can be applied to various catalytic reactions by changing the metal nanoparticle component: dehydrogenation by Pd;[16] hydrogenation and dehydrogenation of N-heterocycles by Pd_2Ru;[17] selective hydrocarbon oxidation by Cu;[18,19] dehydrogenative condensation of secondary alcohols and 1,2-amino alcohols by Ir;[20] chemoselective hydrogenation of nitroarenes by Ni,[21] Co[24] and Fe,[25] and hydrolysis of sodium borohydride by Pt.[23]

In contrast, the design of metal/Si-based composites in nitride matrix systems (*i.e.*, M/Si_3N_4) has never been demonstrated and it remains highly challenging while nitrides can be particularly interesting for catalysis as a support and/or as a catalyst itself.[26–31] This is mainly caused by the reactivity of the central metal cations distributed in the polysilazane network with ammonia (used as atmosphere to form Si_3N_4 from polysilazanes) forming a metal nitride nanophase distributed in the Si_3N_4 matrix. This observation is well illustrated in the recent reports on Si_3N_4-based nanocomposites including TiN/Si_3N_4[32,33] and VN/Si_3N_4[34] compounds. Among them, the TiN/Si_3N_4 nanocomposites exhibited strong synergy with Pt nanoparticles, which were homogeneously deposited in a second synthesis step onto the nanocomposite support. This resulted in excellent catalytic performance for dehydrogenation of sodium borohydride in water.[33] Thus, this report confirmed the attractivity of nitrides for catalysis. To simplify this two-step process, and avoid the use of precious metals such as Pt while forming Si_3N_4 supporting the catalytically active phase (*i.e.*, M/Si_3N_4) in a one-step process, we describe the coordination of a polysilazane (PHPS) with cobalt chloride ($CoCl_2$) allowing the *in situ* formation of Co during the further thermo-chemical conversion of the PHPS into Si_3N_4 in flowing ammonia. The unique low-temperature *in situ* formation of Co within the Si_3N_4 matrix is discussed based on a complete set of characterization techniques including elemental analyses, X-ray diffraction (XRD), thermogravimetric – mass spectrometric (TG–MS) analyses, infrared spectroscopy, ultraviolet-visible (UV-Vis) spectroscopy and transmission electron microscopy

[a] *Department of Life Science and Applied Chemistry, Graduate School of Engineering, Nagoya Institute of Technology, Gokiso-cho, Showa-ku, Nagoya 466-8555, Japan*
[b] *University of Limoges, CNRS, IRCER, UMR 7315, Limoges, F-87000, France*
[c] *Chemical Engineering, Federal University of Santa Catarina, Florianópolis, 88010-970, Brazil*

(TEM) observations. The basis of our approach comes first from the design of a suitable highly pure synthetic precursor in which uniform chemical composition is established at a molecular scale. Thus, we mixed $CoCl_2$ with PHPS which only contains Si, N and H elements in a controlled Co/Si molar ratio of 0.2 to form a compound labeled Co-PHPS. The synthesis is performed in toluene and directed to keep a homogeneous distribution of $CoCl_2$ throughout the PHPS network (without direct reaction). Then, the precursor is heat-treated under ammonia to form an unstable (thermally) metal nitride phase at low temperatures, while avoiding the formation of free Si at higher temperatures as known using PHPS,[35,36] thus leading to Co/Si_3N_4 compounds at low and intermediate temperatures as discussed below.

Pyrolysis leads to samples labeled as Co/SiNX (X being the temperature at which the material has been heat-treated) with tuned phase composition and nano-/microstructure organization according to the pyrolysis temperature. The chemical compositions of the Co/SiNX samples are listed in Table 1. All the procedures for Co-PHPS synthesis, subsequent heat treatment and characterization of Co/SiNX are reported in the ESI.†

Chemical compositions of the Co/SiNX samples are discussed in relation to their XRD patterns (Fig. 1), TG–MS experiments (Fig. 2) and FTIR spectroscopy (Fig. 3). The Co/SiN400 sample exhibits three characteristic diffraction peaks assigned to a-Co (JCPDS No. 00-015-0806 at 2y = 48.6, 52.0, and 55.61) along with a residual component of $CoCl_2$ (JCPDS No. 01-085-0446) and NH_4Cl (JCPDS No. 01-073-0365).

Additionally, two small diffraction peaks appear at 2y angles of 46.5 and 50.41, indicating the formation of cobalt nitride (Co_2N, JCPDS No. 04-004-4638). Then, at 500 1C (Co/SiN500 sample), the Co_2N disappears while the metallic a-Co forms. At 800 1C (Co/SiN800 sample), two distinct diffraction peaks appear at 51.8 and 60.71, which are assigned to b-Co (JCPDS No. 01-089-4308) along with a-Co, and several minor peaks related to both a- and b-Si_3N_4 were also identified. The NH_4Cl XRD peaks disappeared because of its vaporization when heated above 500 1C; this was confirmed by its condensation in the cool parts (extremities) of the furnace tube. Finally, the Co/SiN1000 sample exhibits the formation of thermodynamically favorable cobalt silicide (Co_2Si, JCPDS No. 01-089-4181) in addition to the a- and b-Si_3N_4 phases. Thus, Co/Si_3N_4 (amorphous and crystalline) composites are generated at temperatures below 800 1C. In order to investigate this low-temperature *in situ* formation of a/b-Co, TG–MS analyses have been performed. The TG-curve (Fig. 2a) exhibits two main

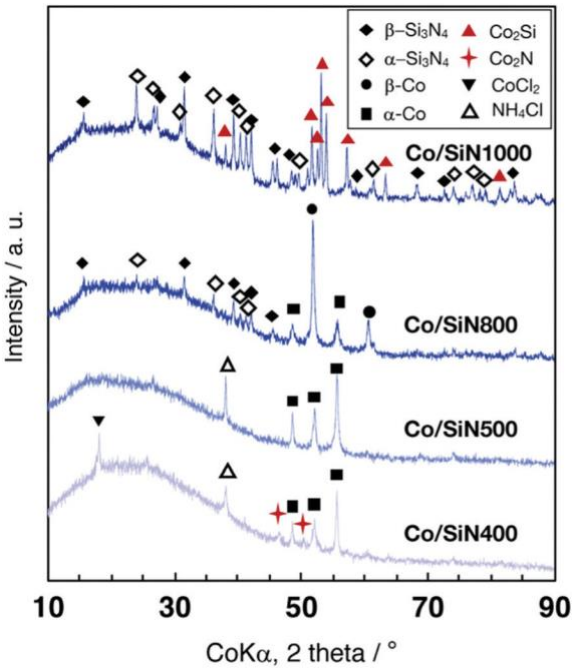

Fig. 1 XRD patterns of Co/SiNX samples.

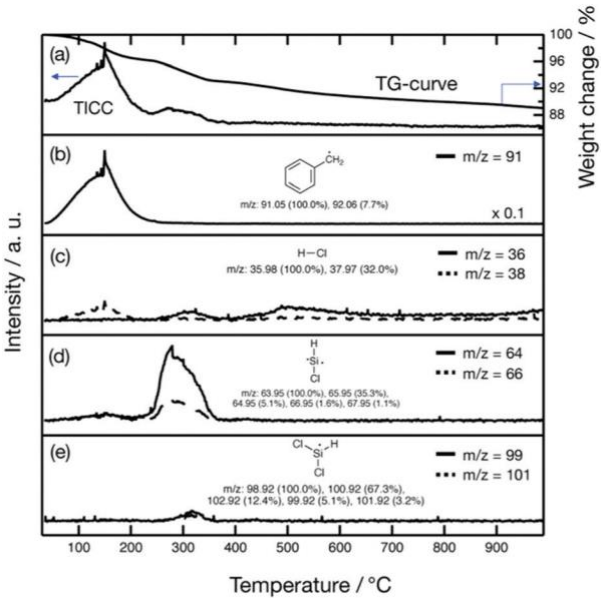

Fig. 2 TG–MS analyses under flowing He of the Co-PHPS sample: (a) a TG-curve and a total ion current chromatogram, (b–e) the simultaneous monitoring of gaseous products formed *in situ*.

Table 1 Chemical composition of the Co/SiNX samples

	Composition/wt%					Composition/at%
	EDS (Co/Si ratio)		Elemental analysis/wt%			
Name	Si	Co	C	N	O	Atomic ratio to Si
CO/SiN400	44.83	35.23	0.80	16.84	2.30	$Si_1Co_{0.37}Co_{0.04}N_{0.75}O_{0.09}$
Co/SiN500	57.40	22.32	0.93	16.36	2.99	$Si_1Co_{0.19}Co_{0.04}N_{0.57}O_{0.09}$
Co/SiN800	52.89	16.70	0.50	23.73	6.18	$Si_1Co_{0.15}Co_{0.02}N_{0.90}O_{0.21}$
Co/SiN1000	53.84	16.08	0.01	26.09	3.98	$Si_1Co_{0.14}Co_{0.00}N_{0.97}O_{0.13}$

weight loss regions at 50–220 1C and 220–350 1C. The coupled MS analysis reveals that the main evolved component at 50–220 1C is toluene ($C_6H_5CH_3$, m/z = 91, Fig. 2b) as the reaction solvent medium, while at 220–350 1C, the dominant gaseous species are chloride fragments, such as hydrochloric acid (HCl, m/z = 36 and 38, Fig. 2c), monochlorosilane (m/z = 64 and 66, Fig. 2d) and dichlorosilane (m/z = 99 and 101, Fig. 2e) species.

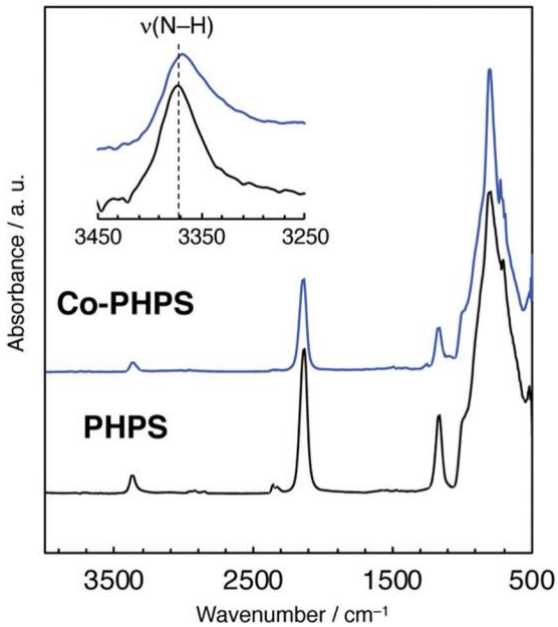

Fig. 3 ATR-IR spectra for the as-received PHPS and Co-modified PHPS.

As shown in Fig. S1 (ESI†), a color change from blue to gray was observed for the $CoCl_2$-dispersed PHPS solution after reflux at 110 1C for 12 h. The visible color change was also monitored by UV-Vis absorption spectroscopy (Fig. S2, ESI†): as-received $CoCl_2$ exhibits a broad peak around 600 nm attributed to octahedral coordination of $CoCl_2$,[37,38] while the Co-PHPS sample recovered after the 110 1C-refluxing in toluene presents
additional absorption bands at 670 and 700 nm assigned to typical bands of tetrahedral coordination which were attributed to the formation of $CoCl_2L_2$ (L = ligands).[37,38] In addition, according to the FTIR spectrum of the Co-PHPS shown in Fig. 3, the characteristic bands at 3370 cm^{-1} (nN–H)[36] of PHPS slightly shift toward lower wavenumber of 3365 cm^{-1}, suggesting the $CoCl_2$ coordination to the NH group of PHPS during the precursor synthesis. We therefore suggest that the reaction between PHPS and $CoCl_2$ better proceeded during the pyrolysis, and the NH_4Cl species detected in the XRD patterns of the Co/SiN400 and Co/SiN500 samples (Fig. 1) are by-products resulting from the nucleation reaction between HCl formed *in situ* and the gaseous NH_3.[39] As shown in Table 1, the Co/Si ratio of the Co/SiN400 sample (0.37) was apparently higher than the nominal Co/Si ratio of Co-PHPS (0.2), which can be explained by the elimination of chlorosilanes at 220–350 1C (Fig. 2(d) and
(e)), *i.e.*, the number of SiH groups decreases. Furthermore, from 400 to 500 1C, the N/Si atomic ratio decreased from 0.75 to 0.57 (Co/SiN500). This corresponds to the reported thermal decom- position of Co_2N at 350–450 1C.[40] Consequently, these results indicate that the following reactions proceed stepwise:

(i) At 220–350 1C, Si–N cleavages in the Co-PHPS sample proceed *via* reaction of the Si center and NH group of PHPS with $CoCl_2$ associated with the elimination of chlorosilanes and HCl to afford Co_2N, respectively.

(ii) At 350–450 1C, Co_2N thermally decomposes to yield metallic-Co.

The N/Si ratio of the Co/SiNX samples in Table 1 increased during pyrolysis from 500 to 1000 1C, indicating the occurrence of nitridation of the evolutive polymer under ammonia above 500 1C.[41] Moreover, the crystallization of Si_3N_4 started at 800 1C, which was approximately 400 1C lower than that of Co-free PHPS-derived amorphous silicon nitride.[36] Table 2 presents the
relationship between the pyrolysis temperature and the average crystallite sizes evaluated for a-Co(101) and b-Co(111). The initial low-temperature crystallization (400 1C) of a-Co yields crystallites of approximately 106 nm. Then, consistent with the pyrolysis temperature, the a-Co nanocrystallites decrease their size *via* phase transformation to thermally favorable b-Co, and the Scherrer analysis indicated an average b-Co nanocrystallite size of 74.4 nm for the Co/SiN800 sample.

To gather micro- and nanostructural information, TEM investigations were performed on the Co/SiN800 sample (Fig. 4). The TEM image of the Co/SiN800 sample (Fig. 4) shows aggregated nanocrystallites with dark contrast and diameter of about 40–80 nm which are embedded in a network with the typical phase contrast of amorphous (or poorly crystallized) materials. The corresponding selected area electron diffraction (SAED) patterns confirm the indexation of both a- and b-Co (inset in Fig. 4). Neither silicon segregations nor inclusions along grain boundaries are observed, while dark spots with several nanometers in size (typical ones are indicated by arrows) are observed which suggested that the crystallite size distribution of Co embedded within the silicon nitride matrix is bimodal: several nanometers and 40 to 80 nm.

In conclusion, the addition of cobalt chloride ($CoCl_2$) on perhydropolysilazane (PHPS) in toluene in a 1/5 molar ratio generated a cobalt-coordinated PHPS that was heat-treated in flowing ammonia in the temperature range of 400 to 800 1C to favor the *in situ* growth of Co nanoparticles in an amorphous silicon nitride matrix. The highlights can be summarized as follows:

(1) Formation of Co_2N formed *in situ* by the reaction of $CoCl_2$ with the Si center and NH group of PHPS at 220–350 1C.

(2) Co started growing at temperature as low as 400 1C *via* the thermal decomposition of Co_2N.

(3) Crystallization of the amorphous silicon nitride matrix proceeded at 800 1C.

Further investigations on the molecular structure of the single-source precursors and subsequent pyrolysis conditions at the low temperatures are still in progress. Therefore, this study paves the way for the rational one-step synthesis of metal/nitride nanocomposites that may be applied in a wide range of catalysis-assisted reactions for energy-related fields. These opportunities are now being addressed. It is anticipated that

Table 2 Relationship between the pyrolysis temperature and the average crystallite sizes evaluated for a-Co(101) and b-Co(111)

	Co/SiN400	Co/SiN500	CoSiN800
a-Co(101)	106	76	29
b-Co(111)	—	—	74

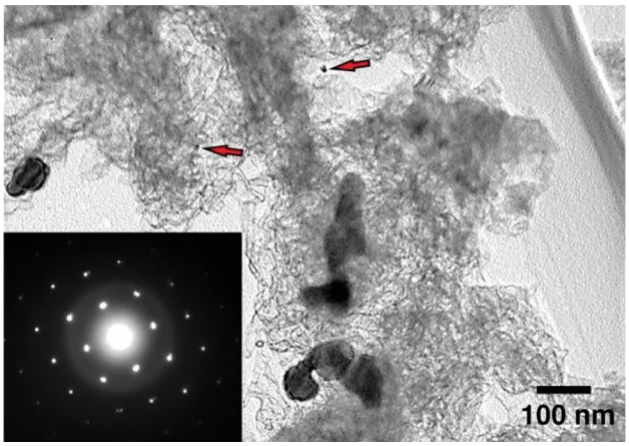

Fig. 4 TEM image of the Co/SiN800 sample, and the corresponding SAED patterns obtained from the aggregated nanocrystallites with dark contrast, and the arrows pointing to several nanometer sized Co crystallites.

this will lead to a host of structural and functional applications for a new generation of advanced ceramics.

This work was partially supported by JSPS KAKENHI Grant Number JP20K05076. Dr Samuel Bernard and Prof. Yuji Iwamoto would like to thank CNRS who financially supported the present work *via* the International Research Project (IRP) 'Ceramics materials for societal challenges'.

Notes and references

1 D. Gielen, F. Boshell and D. Saygin, *Nat. Mater.*, 2016, **15**, 117–120.
2 Y. Zhong, X. Xia, F. Shi, J. Zhan, J. Tu and H. J. Fan, *Adv. Sci.*, 2016, **3**, 1500286.
3 S. Klemenz, J. Schuch, S. Hawel, A.-M. Zieschang, B. Kaiser, W. Jaegermann and B. Albert, *ChemSusChem*, 2018, **11**, 3150–3156.
4 M.-S. Balogun, Y. Huang, W. Qiu, H. Yang, H. Ji and Y. Tong, *Mater. Today*, 2017, **20**, 425–451.
5 E. W. Awin, A. Lale, K. C. H. Kumar, S. Bernard and R. Kumar, *Appl. Surf. Sci.*, 2020, **508**, 144953–144961.
6 M. Eckardt, M. Zaheer and R. Kempe, *Sci. Rep.*, 2018, **8**, 2567.
7 C. Sanchez, C. Boissiere, S. Cassaignon, C. Chaneac, O. Durupthy, M. Faustini, D. Grosso, C. Laberty-Robert, L. Nicole, D. Portehault, F. Ribot, L. Rozes and C. Sassoye, *Chem. Mater.*, 2014, **26**, 221–238.
8 S. Clément and A. Mehdi, *Molecules*, 2020, **25**, 2538–2544.
9 C. Sanchez, L. Rozes, F. Ribot, C. Laberty-Robert, D. Grosso, C. Sassoye, C. Boissiere and L. Nicole, *C. R. Chim.*, 2010, **13**, 3–39.
10 A. Lale, M. Schmidt, M. D. Mallmann, A. V. A. Bezerra, E. D. Acosta, R. A. F. Machado, U. B. Demirci and S. Bernard, *Surf. Coat. Technol.*, 2018, **350**, 569–586.
11 P. Colombo, G. Mera, R. Riedel and G. D. Sorarù, *J. Am. Ceram. Soc.*, 2010, **93**, 1805–1837.
12 E. Ionescu, H. J. Kleebe and R. Riedel, *Chem. Soc. Rev.*, 2012, **41**, 5032–5052.
13 M. Zaheer, J. Hermannsdörfer, W. P. Kretschmer, G. Motz and R. Kempe, *ChemCatChem*, 2014, **6**, 91–95.
14 D. Schumacher, M. Wilhelm and K. Rezwan, *J. Am. Ceram. Soc.*, 2020, **103**, 2991–3001.
15 M. Seifollahi Bazarjani, H. J. Kleebe, M. M. Müller, C. Fasel, M. Baghaie Yazdi, A. Gurlo and R. Riedel, *Chem. Mater.*, 2011, **23**, 4112–4123.
16 D. Forberg, T. Schwob and R. Kempe, *Nat. Commun.*, 2018, **9**, 1751.
17 D. Forberg, T. Schwob, M. Zaheer, M. Friedrich, N. Miyajima and R. Kempe, *Nat. Commun.*, 2016, **7**, 13201.
18 G. Glatz, T. Schmalz, T. Kraus, F. Haarmann, G. Motz and R. Kempe, *Chem. – Eur. J.*, 2010, **16**, 4231–4238.
19 M. Zaheer, T. Schmalz, G. Motz and R. Kempe, *Chem. Soc. Rev.*, 2012, **41**, 5102–5116.
20 D. Forberg, J. Obenauf, M. Friedrich, S.-M. Hühne, W. Mader, G. Motz and R. Kempe, *Catal. Sci. Technol.*, 2014, **4**, 4188–4192.
21 G. Hahn, J.-K. Ewert, C. Denner, D. Tilgner and R. Kempe, *ChemCatChem*, 2016, **8**, 2461–2465.
22 M. Kamperman, A. Burns, R. Weissgraeber, N. van Vegten, S. C. Warren, S. M. Gruner, A. Baiker and U. Wiesner, *Nano Lett.*, 2009, **9**, 2756–2762.
23 S. M. Sachau, M. Zaheer, A. Lale, M. Friedrich, C. E. Denner, U. B. Demirci, S. Bernard, G. Motz and R. Kempe, *Chem. – Eur. J.*, 2016, **22**, 15508–15512.
24 T. Schwob and R. Kempe, *Angew. Chem., Int. Ed.*, 2016, **55**, 15175–15179.
25 C. Bäumler and R. Kempe, *Chem. – Eur. J.*, 2018, **24**, 8989–8993.
26 Y. Han, X. Yue, Y. Jin, X. Huang and P. K. Shen, *J. Mater. Chem. A*, 2016, **4**, 3673–3677.
27 M.-S. Balogun, W. Qiu, W. Wang, P. Fang, X. Lu and Y. Tong, *J. Mater. Chem. A*, 2015, **3**, 1364–1387.
28 W. Yang, S. Rehman, X. Chu, Y. Hou and S. Gao, *ChemNanoMat*, 2015, **1**, 376–398.
29 M.-S. Balogun, Y. Huang, W. Qiu, H. Yang, H. Ji and Y. Tong, *Mater. Today*, 2017, **20**, 425–451.
30 J. S. J. Hargreaves, *Coord. Chem. Rev.*, 2013, **257**, 2015–2031.
31 S. Dong, X. Chen, X. Zhang and G. Cui, *Coord. Chem. Rev.*, 2013, **257**, 1946–1956.
32 M. C. Bechelany, V. Proust, A. Lale, P. Miele, S. Malo, C. Gervais and S. Bernard, *Chem. – Eur. J.*, 2017, **23**, 832–845.
33 A. Lale, M. D. Mallmann, S. Tada, A. Bruma, S. Özkar, R. Kumar, M. Haneda, R. A. Francisco Machado, Y. Iwamoto, U. B. Demirci and S. Bernard, *Appl. Catal., B*, 2020, **272**, 118975.
34 C. Zhou, A. Ott, R. Ishikawa, Y. Ikuhara, R. Riedel and E. Ionescu, *J. Eur. Ceram. Soc.*, 2020, **40**, 6280–6287.
35 M. Biesuz, P. Bettotti, S. Signorini, M. Bortolotti, R. Campostrini, M. Bahri, O. Ersen, G. Speranza, A. Lale, S. Bernard and G. D. Sorarù, *Nanotechnology*, 2019, **30**, 255601.
36 Y. Iwamoto, K. I. Kikuta and S. I. Hirano, *J. Ceram. Soc. Jpn.*, 2000, **108**, 350–356.
37 C. L. Hussey and T. M. Laher, *Inorg. Chem.*, 1981, **20**, 4201–4206.
38 I. Sava, M.-D. Damaceanu and G. Lisa, *J. Polym. Res.*, 2016, **23**, 130.
39 S. Thompson, P. D. Shipman, S. P. Shipman and T. J. Zurlinden, *J. Chem. Phys.*, 2019, **150**, 154306.
40 L. Maya, M. Paranthaman, J. R. Thompson, T. Thundat and R. J. Stevenson, *J. Appl. Phys.*, 1996, **79**, 7905–7910.
41 G. T. Burns and G. Chandra, *J. Am. Ceram. Soc.*, 1989, **72**, 333–337.